ChemPubSoc Europe

DOI: 10.1002/chem.201900975

CHEMISTRY
A European Journal
Concept

Three-Dimensional Printing

Advanced Polymer Designs for Direct-Ink-Write 3D Printing

Longyu Li, Qianming Lin, Miao Tang, Andrew J. E. Duncan, and Chenfeng Ke*[a]

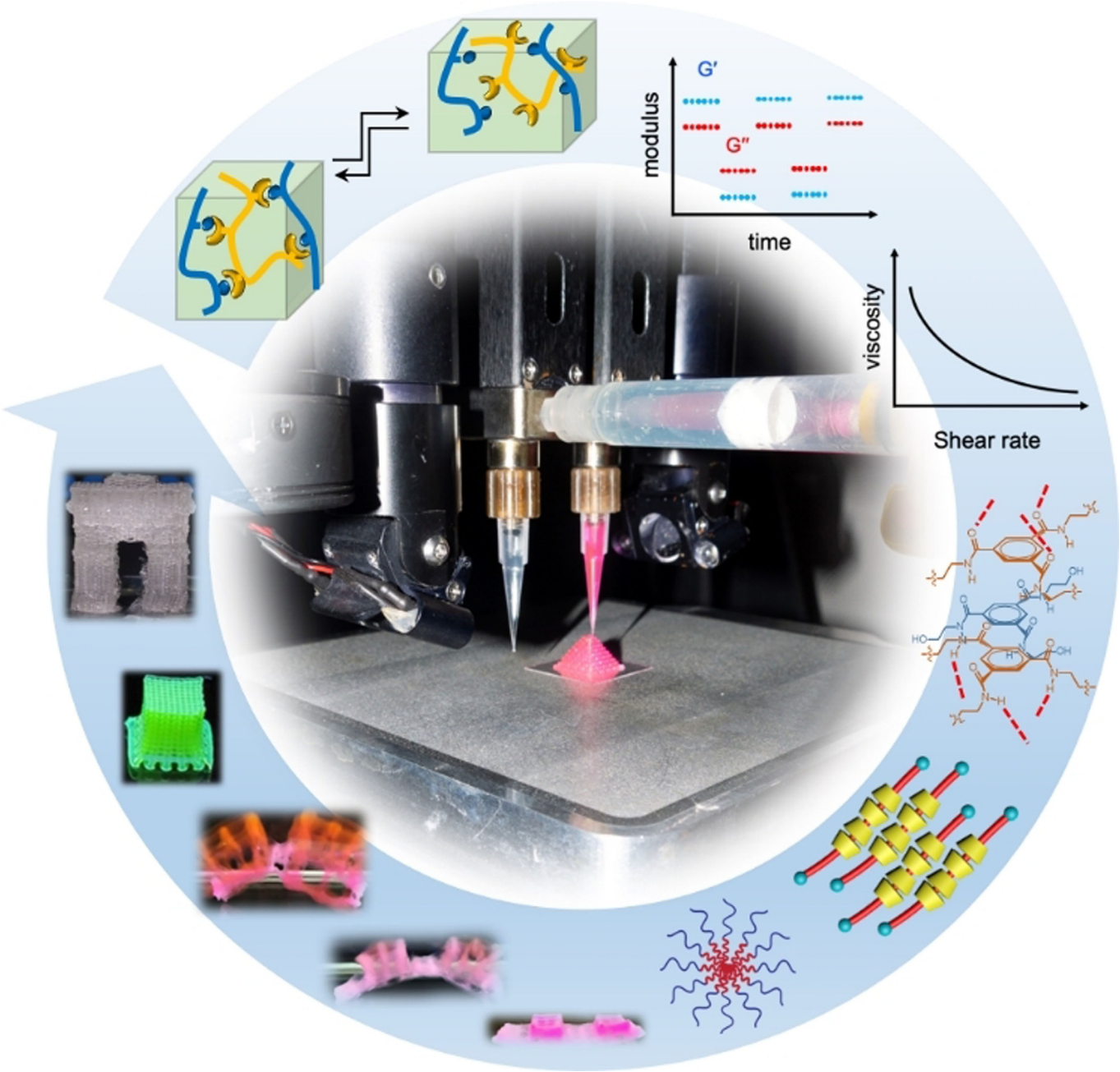

Abstract: The rapid development of additive manufacturing techniques, also known as three-dimensional (3D) printing, is driving innovations in polymer chemistry, materials science, and engineering. Among current 3D printing techniques, direct ink writing (DIW) employs viscoelastic materials as inks, which are capable of constructing sophisticated 3D architectures at ambient conditions. In this perspective, polymer designs that meet the rheological requirements for direct ink writing are outlined and successful examples are summarized, which include the development of polymer micelles, co-assembled hydrogels, supramolecularly cross-linked systems, polymer liquids with microcrystalline domains, and hydrogels with dynamic covalent cross-links. Furthermore, advanced polymer designs that reinforce the mechanical properties of these 3D printing materials, as well as the integration of functional moieties to these materials are discussed to inspire new polymer designs for direct ink writing and broadly 3D printing.

1. Introduction

Additive manufacturing techniques,[1,2] often referred to as three-dimensional (3D) printing, are changing the landscape of polymer chemistry, materials science, and engineering as a result of their ability to rapidly convert advanced digital designs into complex 3D architectures. To date, several 3D printing techniques including extrusion-based fused depositional modeling (FDM),[3–6] stereolithography,[7] and laser-assisted sintering[8] have been successfully commercialized. These 3D printers use polymeric materials, such as thermoplastic filaments, photocurable resins, and polymer powders to rapidly prototype 3D objects for industrial[9] and educational applications.[10] However, the development of additive manufacturing is still in its infancy.[11] On one hand, innovations in new printing methods are in demand for faster and more precise prototyping. On the other hand, the expansion of tailor-made advanced materials for additive manufacturing is critical to unleashing the full potential of 3D printing platforms.[12]

From a polymer design consideration, technical differences between these 3D printing platforms require the use of tailor-designed molecular and polymeric inks. For example, in stereolithographic systems, the ratios of monomers, cross-linkers, and photo-initiators need to be adjusted to allow efficient photo-polymerization, whereas the inhibitor concentrations must also be optimized to limit over-polymerization during the fabrication process.[13] In FDM-based 3D printers, the glass transition temperatures of the thermoplastic filaments must be adjusted within a suitable range (150 to 250 °C).[14] As an ambient temperature alternative technique to FDM, direct ink writing (DIW) employs viscoelastic materials, including polymer liquids,[15] hydrogels,[16] and colloidal suspensions[17] as the printing ink to fabricate advanced 3D architectures. The mild fabrication temperature and the ease of integrating multiple polymer materials make DIW particularly suitable for bio-fabrication, such as constructing tissue regeneration scaffolds[18,19] as well as for the fabrication of soft robotics.[20,21]

In this perspective article, our discussion will focus on polymer designs that facilitate 3D printability for DIW, instead of the broad aspects of the 3D printing techniques and 3D printing materials. We will also discuss polymer designs that reinforce the mechanical robustness of DIW materials, as well as the advanced functions of these 3D printing materials derived from molecular and polymer design.

[a] *Dr. L. Li, Q. Lin, M. Tang, Dr. A. J. E. Duncan, Prof. Dr. C. Ke*
Department of Chemistry, Dartmouth College
41 College Street, Hanover, New Hampshire 03755 (USA)
E-mail: Chenfeng.ke@dartmouth.edu

Supporting information and the ORCID identification number(s) for the author(s) of this article can be found under: https://doi.org/10.1002/chem.201900975.

2. Facilitating 3D printability to polymers

2.1 Rheological pre-requisites for DIW and polymer design considerations

A typical DIW 3D printer (Figure 1 a) possesses two key components: 1) multiple extrusion heads that are controlled by pneumatic pressure or mechanical piston motion and 2) an *xyz* stage to control the deposition path of the printing heads. A photoirradiation system is often conjugated to the printing head for in situ or post-printing polymerization. Successful extrusion in DIW requires the ink to exhibit an adequate reduction of viscosity under applied shear stress (i.e., shear thinning) (Figure 1 b). Similar to injectable inks,[22–24] an empirical ink viscosity range between 0.1 to 10^3 Pa s^{-1} is suggested as suitable for DIW.[25–27]

One distinctive feature of DIW inks in contrast to injectable inks is their ability to rapidly self-heal after extrusion. That is, the ink flows with a lower viscosity (loss modulus $G'' >$ elastic modulus G') under a shear force, but rapidly recovers its mechanical properties ($G'' < G'$) after the shear force is removed (Figure 1 c). In this case, a fast moduli recovery, rather than a slow but efficient moduli recovery, often measures the success of DIW as most extrusion heads travel at a speed of several millimeters per second. Empirically, a self-healed elastic modulus G' of the ink that exceeds 10^3 Pa can support a high-profile stable 3D structure (more than two vertical layers), and the difference between the elastic and loss modulus of the recovered ink needs to be large enough (we suggest $G''/G' < 0.8{:}1$). Therefore, the design considerations that facilitate 3D printability for DIW should be largely focused on their self-healing behaviors,[28–30] because shear-thinning properties are widely found in polymer liquids,[31] hydrogels,[32] and other soft materials.[33] Taking a viscous solution of a linear polymer as an example, under applied mechanical stress the randomly coiled polymer chains are disentangled, resulting in a viscosity decrease. When the external stress is removed, the polymer chains recoil to maximize the entropy.[34,35] In most cases, this recovery process is too slow (several minutes to hours) to be practical for DIW (Figure 1 d).

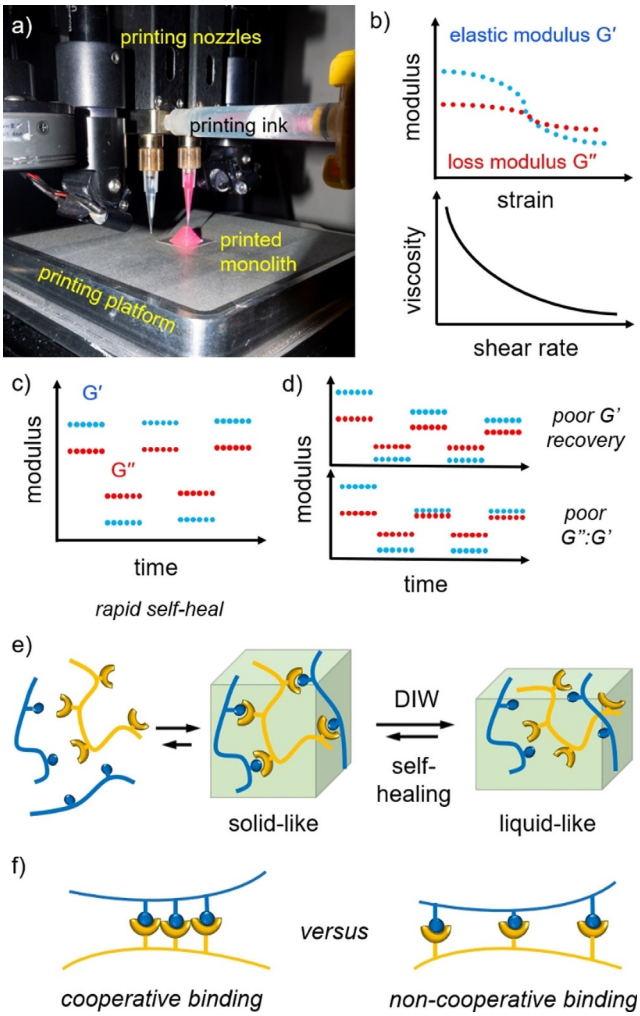

Figure 1. a) A direct-ink-write 3D printing system equipped with two extrusion nozzles. b,c) Desired rheological properties of a typical DIW polymer, which possess b) shear thinning and c) rapid self-healing properties. d) Stress-strain measurements of inks with poor self-healing. e) Illustration of the design of a 3D-printable polymer. f) Illustration of a cooperative multivalent binding event and a non-cooperative multivalent binding event.

Intrinsically, the self-healing properties of polymers could be promoted by installing multivalent non-covalent or dynamic covalent interacting motifs to the polymer chain.[36–38] During the extrusion process, the viscosity of the polymer material decreases upon mechanical shearing and the multivalent interactions are disrupted. When the shear force is removed, these dynamic cross-links rapidly re-establish and the polymer material will recover its macroscopic elastic moduli (Figure 1e). A variety of supramolecular interacting motifs binding through metal–ligand coordination,[39–41] hydrogen bonding,[42–44] electrostatic interaction,[45–47] van der Waals interaction[48,49] (with phase separation), and hydrophobic effects[50,51] are suitable for the design of DIW-compatible polymers. Increasing the number of supramolecular cross-linkers on the polymer backbone will not only accelerate the rate of self-healing but also increase the viscosity and elastic moduli of the ink.

One often overlooked consideration in the supramolecular polymer design is the control of the kinetics of association and dissociation between the supramolecular cross-linkers, which impacts the loss modulus of the polymer material.[52] Sometimes, polymers with multivalent supramolecular cross-linking motifs could not maintain their 3D printed structure, and successful 3D printing was aided by the addition of a colloidal rheological modifier,[53,54] by printing into a supporting matrix,[55,56] or by in situ photo-induced cross-linking.[57,58] In these inks, the difference between the recovered elastic and loss moduli is often small, suggesting the supramolecular cross-linking motifs of the polymer are rapidly exchanging at the molecular level. The fast cross-linker exchange of the polymers exhibits as 3D structure deformation over time at the macroscale. To slow down the cross-linker exchange and stabilize the 3D printed architecture at the macroscale, these binding motifs should be installed in close proximity on the polymer backbone rather than sparsely distributed, as a cooperative multivalent binding[59,60] can effectively localize the cross-linker exchange (Figure 1f).

Another general strategy to reinforce the extruded polymer materials as stable 3D architectures is extrinsically increasing the elastic moduli of the extruded inks. A number of methods, including chemical cross-linking, interfacial stabilization, and providing physical support have been demonstrated successful in introducing novel polymeric materials into DIW. Hence, we divide our discussions into two sections.

2.2 Intrinsic self-healing polymer designs for DIW

Although natural polymers, such as gelatin,[61,62] have been demonstrated with good rheological properties for DIW, this section is focused on designing synthetic polymers to tailor their intrinsic rheological properties, particularly rapid self-healing, for DIW. The ink compositions and 3D printing technical specifications discuss below are summarized in Table S1 in the Supporting Information.

Micellar hydrogels

Amphiphilic molecules and polymers are known to form micellar aggregates in aqueous environments as a result of hydrophobic effects.[63] When the concentration of an amphiphile reaches the critical gelation concentration, these micelles further aggregate to form interconnected 3D networks to afford a viscoelastic hydrogel.[64,65] Upon shearing, the high-order 3D micellar structure of the hydrogel is disrupted, resulting in a decrease in viscosity. After the removal of shear force, the interconnected 3D micellar structure quickly recovers under thermodynamic control (Figure 2a). For example, a triblock copolymer of pluronic F127 possessing a hydrophobic polypropylene oxide (PPO) core and two hydrophilic polyethylene oxide (PEO) tails forms spherical micelles in aqueous solution. Increasing the concentration of F127 to 21 w/w% affords a viscoelastic hydrogel at 25 °C that is suitable for DIW.[66] Zhao et al. systematically evaluated[67] the 3D printability of F127-based hydrogels at different concentrations (Figure 2b). They reported an optimum hydrogel concentration range of 18–36 wt% for a telechelic diacrylate derivative of F127 (F127-DA). To invert the

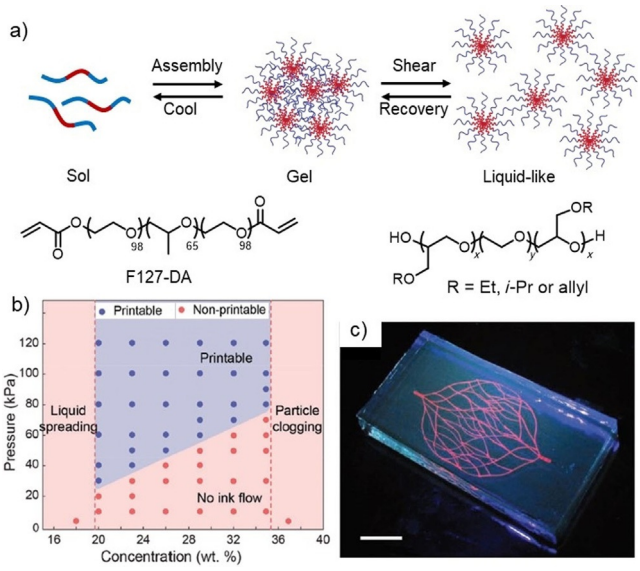

Figure 2. a) Schematic illustration of shear thinning, self-healing, and thermo-responsive behaviors of micellar hydrogels formed by amphiphilic triblock copolymers. b) 3D-printability diagram of F127-DA hydrogels. Reproduced with permission from reference [67]. Copyright 2018 John Wiley & Sons, Inc. c) Fluorescent image of a 3D microvascular network fabricated by printing a fugitive ink (red) into an F127-DA matrix (scale bar: 10 mm). Reproduced with permission from reference [71]. Copyright 2011 John Wiley & Sons, Inc.

hydrophobic and hydrophilic segments of the amphiphilic polymer, Nelson et al. reported a series of triblock copolymers (P*i*PrGE-*b*-PEG-*b*-P*i*PrGE) composed of a polyethylene glycol (PEG) core and two poly(isopropyl glycidyl ether) (P*i*PrGE) tails (Figure 2a).[68,69] These copolymers aggregate in aqueous solutions to form micelles. When the concentration of P*i*PrGE-*b*-PEG-*b*-P*i*PrGE reaches 14 w/w%, 3D printable viscoelastic hydrogels were obtained. Photoirradiation of the micellar F127-DA hydrogel and the P*i*PrGE-*b*-PEG-*b*-P*i*PrGE hydrogel with thiol cross-linkers affords robust, chemically cross-linked 3D monoliths.

Some of these micellar hydrogels possess an interesting temperature-gated sol–gel transition behavior.[64,70] For example, an F127 hydrogel at room temperature will be converted to a liquid phase when the temperature is decreased below its critical gelation temperature. At a lower temperature, the previously hydrophobic PPO segment is solvated by water molecules and the F127 micelles are converted to a solution of F127 polymers. Taking advantage of this temperature-controlled sol–gel transition behavior, Lewis et al. developed[71] a method to 3D print biomimetic microvascular networks by using a F127 hydrogel as a fugitive (sacrificial) ink and a F127-DA hydrogel as a scaffolding gel. As shown in Figure 2c, F127 ink was printed into a reservoir of F127-DA hydrogel followed by UV irradiation. The F127-DA hydrogel was cross-linked and the F127 ink remains intact. When the temperature is decreased, the fugitive F127 hydrogel was converted to a flowing liquid, which was subsequently removed to generate the 3D microvascular network. This method has been expanded by the same group to fabricate soft somatosentitive actuators[72] and 3D vascularized proximal tubule models for renal tissue regenerations.[73]

Another feature of these amphiphilic micellar hydrogels is their ability to form inclusion complexes and supramolecular co-assemblies with small molecules and polymers.[74,75] Interestingly, the properties of the co-assembled hydrogels resemble the viscoelastic behaviors of the micellar hydrogels used for 3D printing. By utilizing this feature, we reported a hierarchical co-assembly-enhanced DIW method[76] and successfully integrated functional small molecules into 3D printing inks (Figure 3a). In these hydrogels, inorganic monomers, such as tetraethyl orthosilicate (TEOS), and organic monomers, such as benzene-1,3,5-tricarboxamide (BTA) derivatives, co-assemble with F127 micelles in water. Although the superstructures of these co-assemblies are disrupted during the extrusion process, after DIW a carefully controlled evaporation-induced co-assembly process reconstructs and further refines the superstructures of these co-assemblies at the nanoscale. Chemically cross-linking the monomers followed by removal of F127 affords functional 3D printed monoliths that are composed of the ordered small molecular entities only. For example, the lattice cube fabricated by using TEOS/F127 ink shrank to 2% of

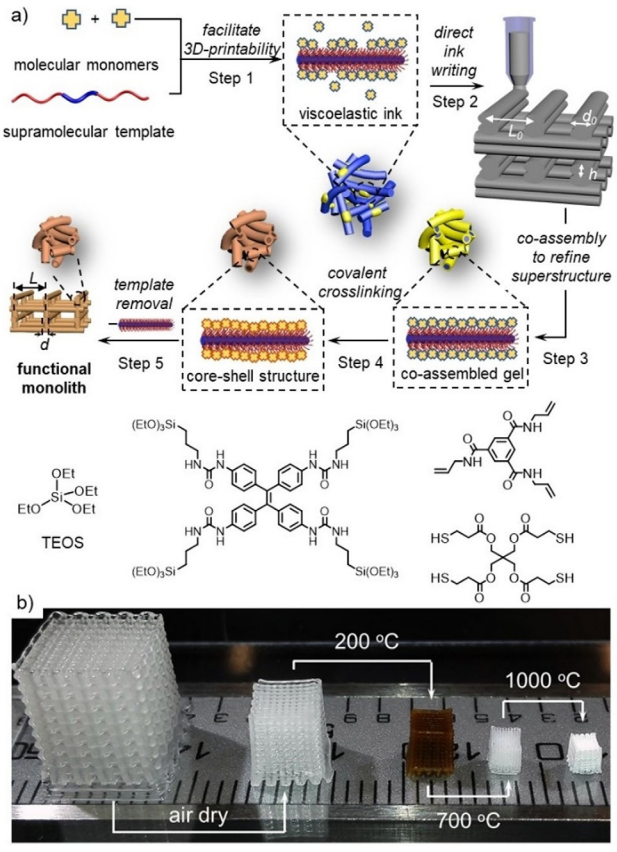

Figure 3. a) Design of hierarchical co-assembly-enhanced direct ink writing. The ink is formed by co-assembling molecular monomers with a supramolecular template. After DIW, evaporation-induced co-assembly, covalent crosslinking, and template removal functional monoliths with enhanced printing resolution and preserved molecular functions are obtained. b) Woodpile lattice cubes ($9.0\times9.0\times9.6$ mm^3) printed and calcinated at 200, 700, and 1000 °C, respectively. Reproduced with permission from reference [76]. Copyright 2018 John Wiley & Sons, Inc.

its original size, which not only improves the DIW printing resolution by an order of magnitude but also imparts high structural integrity across the nano- to macroscale (Figure 3b). When BTA monomers are integrated into the co-assembly ink, the BTA entities retained their hydrogen-bonded superstructure. When another BTA derivative was introduced to and removed from the 3D printed BTA monolith, the lattice expanded and contracted as a result of the supramolecular insertion.

Multivalent supramolecular interactions

The dynamic nature of supramolecularly cross-linked polymers,[77–79] where the non-covalent interactions are disrupted upon shearing and are re-established after removal of the shear force, renders them particularly amenable to DIW. Although most non-covalent interactions are, in principle, suitable for the design of supramolecular 3D printing polymers, their binding thermodynamics and kinetics must be tailored for DIW, that is, the (re)association kinetics of these non-covalent interactions must be fast (within milliseconds) to allow rapid structural reformation after 3D printing. Among them, introducing metal–ligand coordination networks and host–guest auxiliaries are demonstrated methods to facilitate the self-healing properties in polymers for DIW.

For example, when the naturally occurring biopolymer alginate is mixed with Ca^{2+} salts, multivalent coordination is established between the carboxylate groups of alginate and the metal cations, affording a viscoelastic hydrogel.[80,81] Shu et al. developed[55] a multi-step method to 3D print complex, cell-laden alginate hydrogel structures with good mechanical properties (Figure 4a). A partially Ca^{2+}-cross-linked alginate hydrogel was prepared by using 4 wt% of alginate and 0.4 wt% of $CaCl_2$ for DIW. The extruded structure was gradually immersed in a solution of $CaCl_2$ during the DIW process to increase the supramolecular cross-linking density, thereby forming a robust self-supportive 3D architecture. When the printed monolith was soaked in a solution of $BaCl_2$, the elastic modulus of the hydrogel increased significantly, which may be attributed to a stronger supramolecular cross-linking realized by the Ca^{2+}-to-Ba^{2+} exchange.

Burdick et al. appended[56] β-cyclodextrin (β-CD) and adamantane (Ad) motifs to hyaluronic acid (HA), affording two side-chain polymers, HA-β-CD and HA-Ad, in which 25–40% of HA repeat units are chemically modified with β-CD and Ad, respectively (Figure 4b). When HA-β-CD and HA-Ad are mixed in a 1:1 ratio at a total concentration of 5 wt/v%, a viscoelastic hydrogel with shear-thinning and self-healing properties is obtained. The loss moduli of the hydrogel, however, are too close to the elastic moduli to be self-supportive for DIW. This obstacle was cleverly bypassed through a gel-in-gel printing method, which will be discussed in detail later. Meanwhile, a secondary methacrylate cross-linking moiety (≈20% of repeat units of HA) was conjugated to the HA component polymers, allowing for photo-cross-linking of the gel-in-gel-printed material and the successful fabrication of a stable, freestanding 3D architecture.

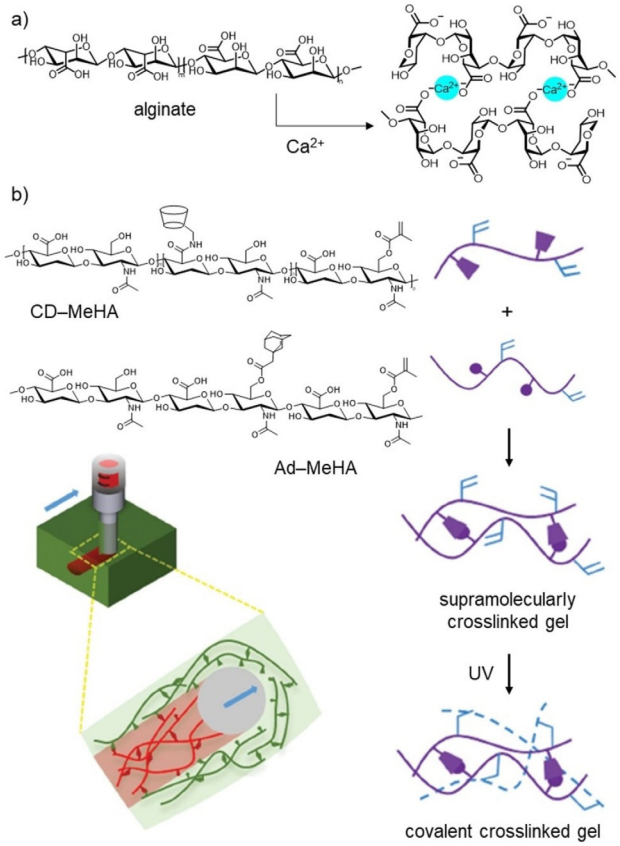

Figure 4. a) Formation of an alginate–Ca^{2+} hydrogel. b) Hydrogels formed by printing of HA-Ad and HA-β-CD polymers with methacrylate groups into a gel matrix followed by photo-crosslinking to afford the desired 3D architecture. Reproduced with permission from referene [56]. Copyright 2015 John Wiley & Sons, Inc.

Micro-crystallization

Although micro-crystallization of polymers has been demonstrated as a promising means to generate sophisticated supramolecular 1D,[82,83] 2D,[84,85] and 3D[86,87] architectures, utilizing the technique to facilitate 3D printability is largely under-developed. Similar to viscoelastic micellar hydrogels, the microcrystalline domain of a polymer can be disrupted by mechanical shear force and re-established after the removal of the shear force. Likewise, a fast re-crystallization process is desired to allow rapid self-healing of the polymer material, thereby facilitating 3D printability for DIW. Recently, Wu et al. developed[88] a 3D printable hydrogel, which was prepared through a micellar copolymerization of *N*,*N*-dimethylacrylamide (DMA) with *n*-octadecyl acrylate (C18). The C18 side chains of the polymer form microcrystalline domains as reversible cross-links. In order to allow DIW, the ink was heated to 45 °C to disrupt the microcrystalline domains and decrease the viscosity. When the ink was deposited onto a platform with a temperature of 10 °C, the crystalline domains recovered quickly, affording a 3D printed grid-structured hydrogel for the fabrication of skin-like capacitance devices.

We introduced the microcrystallization of cyclodextrin (CD)-based polypseudorotaxanes to develop DIW inks with mechan-

ically interlocked architectures.[89,90] In this design, 3D printable polypseudorotaxane inks are composed of ring component α-CDs and axle component PEO or F127. In an aqueous solution, α-CD rings thread onto the axle to form a tubular polypseudorotaxane (Figure 5a) driven by ring–ring hydrogen-

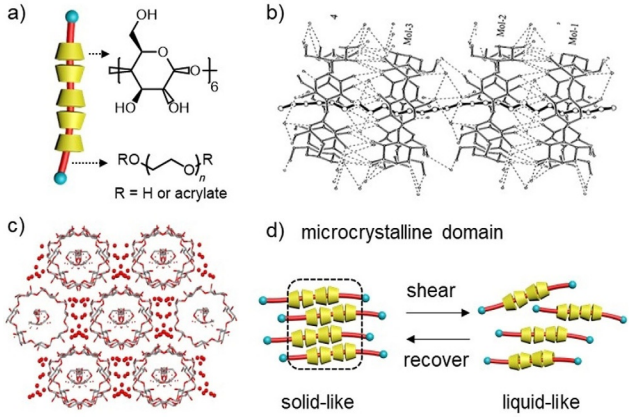

Figure 5. a) Illustration of a polypseudorotaxane formed by α-CD and PEO, where α-CD units are threaded on the PEO axle to form tubular structures. b) Crystal structure of a polypseudorotaxane formed by β-CD and poly(trimethylene oxide), where the dash lines represent hydrogen bonds. Reproduced with permission from reference [91]. Copyright 2000 American Chemical Society. c) Hexagonal packing of polyrotaxane tubular structures in the solid state with included water molecules (red dots). d) Graphical representation of the shear-thinning and self-healing behaviors of a polypseudorotaxane hydrogel, where the inter-tubular hydrogen-bonding network is disrupted upon shearing and recovered after the shearing.

bonding interactions (Figure 5b), thermodynamically favored ring–axle interactions, and the release of high-energy water in the CD rings. These tubular polypseudorotaxanes then crystallize through water-mediated hydrogen-bonding interactions,[91] forming hexagonally packed microcrystalline domains in the aqueous environment (Figure 5c). We discovered that the 3D printability (shear thinning and rapid self-healing properties) (Figure 5d) of these polypseudorotaxane hydrogels is dictated by two parameters: the axis polymer chain length and the number of CD rings. The 3D printable hydrogels were prepared by adding a large amount of CD to a dilute solution of PEO ($40\,000 > M_n > 10\,000$ Da). When telechelic PEO with acrylate end groups is employed as the axle polymer, photo-crosslinking of the acrylate groups affords free-standing polyrotaxane monoliths. Although 3D printing inks designed under this principle are still rare, we foresee that similar microcrystallization-enabled 3D printing polymers will emerge along with the rapid advancement of the development of 3D printing polymers.

Dynamic covalent chemistry

The reversible nature of dynamic covalent reactions, including imine condensation and boronic ester formation, makes them amendable for DIW polymer design. Dynamic covalently cross-linked polymers with outstanding self-healing properties have demonstrated the ability to recover from physical damages and restore functionalities.[92,93] Compared to supramolecular cross-linking, the disruption and recovery of dynamic covalent bonds are considerably slower, however, as the bonding enthalpy of covalent bonds is much higher than non-covalent interactions, restoring even a fraction of the dynamic covalent bonds may allow the extruded polymers to support the 3D architecture for successful DIW (Figure 6a). For example, Connal

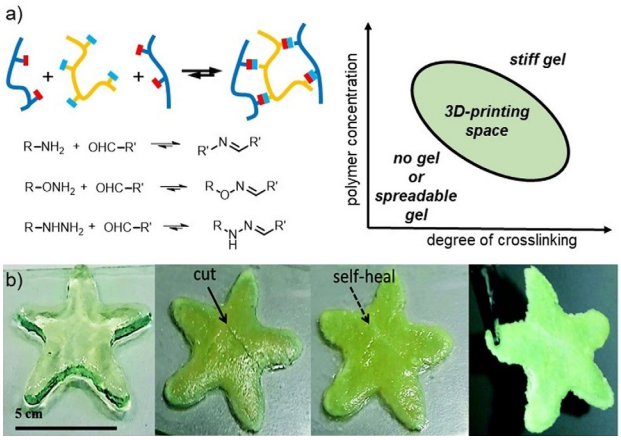

Figure 6. a) Illustration of the formation of 3D printable gels crosslinked by dynamic covalent bonds, including imine, oxime, and hydrazone moieties. b) Images of a star-shaped hydrogel after 3D printing, manual cutting, 1 h of self-healing, and drying at ambient conditions (left to right). Reproduced with permission from reference [94]. Copyright 2017 The Royal Society of Chemistry.

et al. synthesized[94] benzaldehyde-functionalized poly(2-hydroxyethyl methacrylate) (PHEMA) polymers and mixed them with ethylenediamine (EDA) as a cross-linker. By varying the polymer concentrations and the degree of cross-linking, a series of inks with different viscosities and storage moduli was obtained and the optimized gel with balanced rheological properties was 3D printed successfully. They later reported a 3D printable oxime hydrogel formed through cross-linking poly(*n*-hydroxyethyl acrylamide-co-methyl vinyl ketone) with a bifunctional hydroxylamine (Figure 6b).[95] Burdick et al. reported[96] a hydrazone-based 3D printable hydrogel by cross-linking hydrazide-modified hyaluronic acid and aldehyde-modified hyaluronic acid. To improve the mechanical robustness of the 3D printed architecture, a secondary polymer network was introduced to the gel, which increased the elastic moduli of the gel by an order of magnitude (500 Pa to 5 kPa).

When the dynamic covalent cross-linking density is high, the viscosity of the ink may be too high to extrude. A modified dynamic covalent cross-linking method[97] was demonstrated by gradually introducing dialdehyde cross-linkers through an enzyme-catalyzed reaction. In this ink, amino-polysaccharides, dibenzylamine-PEG, H_2O_2 catalase, and the enzyme monoamine oxidase B (MAO B) are mixed together. In the presence of H_2O_2 catalase, MAO B actively converts the dibenzylamine-PEG to dialdehyde-PEG, the latter subsequently cross-linking the polysaccharides. This 3D printed hybrid monolith is responsive to biological stimuli, such as lysine, which gradually de-

grade the cross-linked imine network in biologically relevant environments.

Future polymer design considerations

It is summarized above that the reported polymers for successful DIW possess good shear-thinning and rapid self-healing properties. One important consideration to facilitate the 3D printability of these polymers is increasing the effective multivalent interactions between polymers at the molecular level to accelerate the self-healing process. Methods, including micellar gel formation, introducing supramolecular and dynamic covalent cross-linking, as well as microcrystallization, have been successfully introduced as advanced polymers to DIW. It is also worth noting that the rate of self-healing is also dependent on the shearing rate experienced during the extrusion process. This phenomenon is particularly noticeable in phase-separation-induced self-healing polymers (e.g., microcrystallization-enabled DIW as discussed above). When a high shear rate is applied to these inks, the sizes of the microcrystalline seeds in the inks are significantly reduced, which extends the phase-separation time and slows the self-healing process. Practically, the shear rate of the DIW process needs to be optimized for successful 3D printing.

2.3 Extrinsically reinforced extruded inks in three dimensions

Although many polymers can be extruded from the nozzle of a DIW printer, their viscoelastic properties cannot support their structures in three dimensions. This section focuses on methods that bypass the rheological requirements.

In situ cross-linking-assisted 3D printing

Apart from tailoring the viscoelastic behavior of polymers, in situ chemical cross-linking of an extrudable ink is another way to 3D print polymers into complex architectures. The chemical principles underlying this method are similar to those in the design of inks for stereolithography, but the mild processing conditions and compatibility with bio-inks make in situ cross-linking-assisted DIW particularly attractive for regenerative medicine.

Incorporating photo-cross-linking moieties into injectable gels and polymerizing them is the method that has been predominantly explored for DIW.[98–101] The 3D printer is equipped with a light source (often a UV lamp) and inks are extruded through a transparent printing nozzle. In contrast to post-printing photo-cross-linking, when the polymerization takes place simultaneously along extrusion, the viscosity of the ink increases along the printing nozzle. Therefore, the rate of photo-cross-linking needs to be engineered carefully so that the polymerization is not too fast to clog the printing tip but rapid enough to form mechanically robust inks that are self-supportive. When methacrylated hyaluronic acid is employed as a model ink, three photo-cross-linking scenarios, including pre-printing cross-linking, in situ cross-linking, and post-printing cross-linking, are compared in parallel.[57] When the ink is exposed to UV radiation prior to extrusion, the viscosity of the gel increases, resulting in heterogeneous structures with high and inconsistent extrusion force. In the post-printing cross-linking example, the ink could not maintain the structural integrity of the 3D structure. In the in situ polymerization scenario, the light intensity and ink travel velocity are carefully optimized to afford uniform filament structures that are self-supportive. Other injectable inks consisting of gelatin methacryloyl (GelMA), poly(ethylene glycol) diacrylate (PEG-DA), or norbornene-functionalized HA (NorHA) were also polymerized to afford bio-compatible scaffolds (Figure 7 a).

In a similar manner, Long et al. reported[102] the additive manufacturing of thermoset polyimides (also known as Kapton) through this in situ cross-linking-assisted DIW. The extrudable ink is composed of polyamic acid (PAA) and 2-(dimethylamino)ethyl methacrylate (DMAEMA), which adjusts the rheological properties of the ink for extrusion (Figure 7 b). After

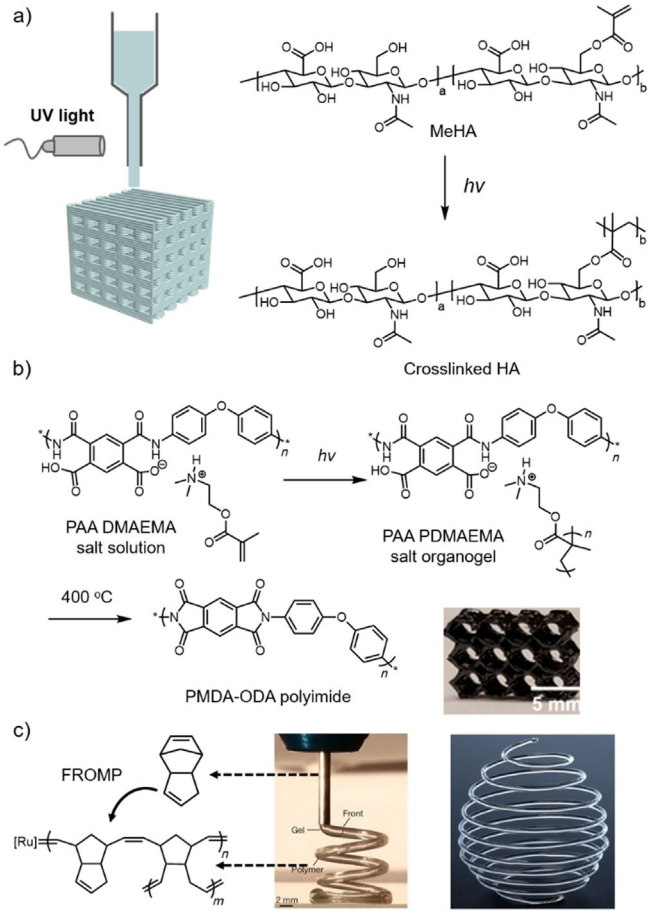

Figure 7. a) A MeHA hydrogel was photo-cross-linked during the extrusion process to form a mechanically robust 3D architecture. b) A viscous solution of a PAA/PMAEMA complex was extruded and photo-polymerized simultaneously to generate a polyamide monolith, which was subsequently heated to induce imide formation. Reproduced with permission from reference [102]. Copyright 2018 American Chemical Society. c) Dicyclopentadiene monomers are polymerized by frontal ring-opening metathesis polymerization (FROMP) through DIW to form free-standing cross-linked structures. Reproduced with permission from reference [103]. Copyright 2018 Macmillan Publishers, Nature.

in situ cross-linking-assisted DIW, the amide polymer monolith was heated to an elevated temperature to induce an amide-to-imide transformation, affording polyimide 3D objects that are otherwise difficult to fabricate by using conventional methods.

Instead of using external stimuli to trigger the polymerization, White et al. introduced[103] frontal polymerization to cross-link monomers during DIW. Frontal polymerization is a self-propagating exothermic reaction where the polymerization-generated heat subsequently initiates the surrounding monomers.[104,105] The frontal-polymerization-based ink is composed of three key compounds: 1) a dicyclopentadiene as the monomer for ring-opening metathesis polymerization, 2) a second-generation Grubbs catalyst that can be thermally activated, and 3) an alkyl-phosphite inhibitor with optimized concentration to control the polymerization rate and subsequently the rheological profile of the ink.[106] When the ink is deposited onto a heated substrate, the ring-opening metathesis polymerization is initiated and the heat wave generated by the frontal exothermic reaction polymerizes the following extruded monomers. This way, the viscous monomers extruded from the printing nozzle are polymerized continuously to afford rigid and sophisticated 3D architecture without the requirement of a supporting matrix (Figure 7c). It is important to note that the printing velocity needs to be tailored to match the rate of the frontal polymerization to prevent frontal quenching.

3D printing enabled by the external environment

A common method to bypass rheological constraints is gel-in-gel 3D printing. In general, a polymer ink is extruded into a supporting gel to stabilize their 3D architectures (Figure 8a). The method is often coupled with a post-printing cross-linking on the writing gel or the supporting gel. For example, Feinberg et al. developed a thermo-responsive supporting matrix for a gel-in-gel printing by breaking the gelatin hydrogels into micrometer-sized particles.[15] Angelini et al. prepared assembled micro-organogels as the supporting matrix,[107] and fine-tuned the ratios of the two block copolymers to adjust their rheological property to enable gel-in-gel DIW. Heating the supporting gel above 60 °C induced a gel-to-liquid phase transition, which released the 3D printed object from the supporting matrix. Although polymeric species in these gels have small diffusion coefficients, small molecular species can quickly diffuse in/out from the writing/support gel, which limits their use in specific applications.

Printing injectable inks into a solution-based supporting matrix is less popular as a result of the challenge of diffusion control. At the turn of the millennium, Lewis and Gratson injected[108] concentrated polyelectrolyte complex inks composed of polyacrylic acid and polyethyleneimine into a reservoir of an alcohol/water mixture to induce coagulation. When the ink was deposited into the reservoir, the polyelectrolyte complex rapidly solidified to support its 3D architecture. Writing alginate inks into a calcium solution produces a Ca^{2+}/alginate gel, however, the printing speed needs to be optimized carefully to avoid tip clogging.[109] In addition to reinforcing the ink through coagulation or coordination, Yin et al. demonstrated

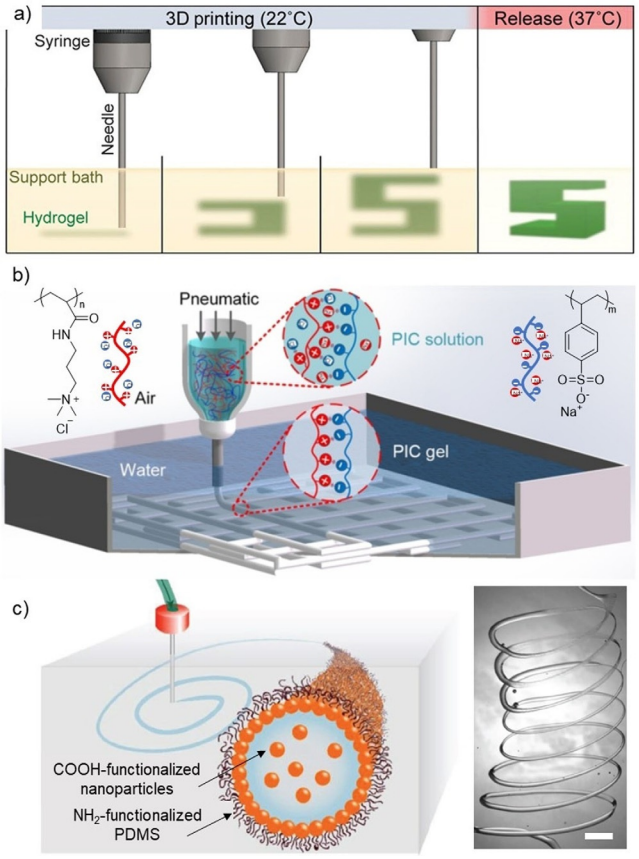

Figure 8. a) Schematic illustration of a gel-in-gel printing by extruding biologically relevant hydrogel inks including alginate, fibrin, collagen type I, and Matrigel (green) into a supporting bath (yellow) composed of gelatin microparticles. The 3D printed object is released by heating the gelatin supporting matrix to 37 °C. Reproduced with permission from reference [15]. Copyright 2015 American Association for the Advancement of Science. b) A viscous polyelectrolyte solution composed of poly(3-(methacryloylamino)-propyl-trimethylammonium chloride) (PMPTC) and poly(sodium *p*-styrenesulfonate) (PNaSS) with high sodium concentration was extruded into a water bath to form a stable 3D architecture. Reproduced with permission from reference [110]. Copyright 2016 American Chemical Society. c) An aqueous solution of carboxylic acid-functionalized nanoparticles (20 nm diameter) was extruded into an oil bath containing 5 w/w% mono-aminopropyl-terminated poly(dimethylsiloxane) (PDMS-NH_2), forming a liquid-in-liquid 3D architecture stabilized through a jammed water/oil interface (scale bar: 2 mm). Reproduced with permission from reference [111]. Copyright 2018 John Wiley & Sons, Inc.

that the electrostatic interactions between polyelectrolyte complexes in the ink could be shielded by using a high concentration of salts (Figure 8b).[110] When liquid-like polyelectrolyte complexes are deposited into water, the salts quickly diffused into the aqueous environment and the electrostatic interactions between the polycations and polyanions recovered to afford a free-standing 3D architecture. They noted that the polymer concentration plays a critical role to realize 3D printing, where too high concentrations of polymers increase the viscosity to a non-extrudable range and too low concentrations of polymers does not allow gelation.

Different from gel-in-gel or gel-in-solution DIW, Russell et al. developed a unique liquid-in-liquid 3D printing method by chemical control of the liquid/liquid interface (Figure 8c).[111]

This method is based on their discovery that non-spherical fluid drops could be obtained by stabilizing the liquid/liquid interface through interfacial jamming of nanoparticles.[112] When an aqueous solution of carboxylic acid-functionalized nanoparticles was extruded into a mono-aminopropyl-poly(dimethylsiloxane) (PMDS-NH_2)-containing silicone oil bath,[111] the negatively charged carboxylic acid-functionalized nanoparticles bind the PMDS-NH_2 at the oil/water interface, forming elastic assemblies of nanoparticle surfactants (NPSs) that stabilized the extruded filament shape.

Comparisons between intrinsically and extrinsically stabilized 3D printed polymers

In order to obtain a robust 3D architecture, most 3D printed monoliths constructed by self-healing polymers require a secondary cross-linked network, which is often achieved by post-printing photo- or thermo-polymerization. This feature allows chemists to refine the superstructures of the 3D printed polymers at the molecular level (through post-printing self-assembly) before the establishment of the secondary cross-linking network. In contrast, mechanically robust and kinetically cross-linked networks are rapidly generated during the 3D printing process in those extrinsically stabilized 3D printing polymers, which simplify the additive manufacturing process. However, most existing designs to extrinsically stabilize the 3D printed polymer require customized 3D printing platforms (e.g., special photoirradiation head, printing nozzle, printing bed, and etc.) and fine-optimization of the inks. Depending on specific applications, tailored polymer designs should be considered as discussed below.

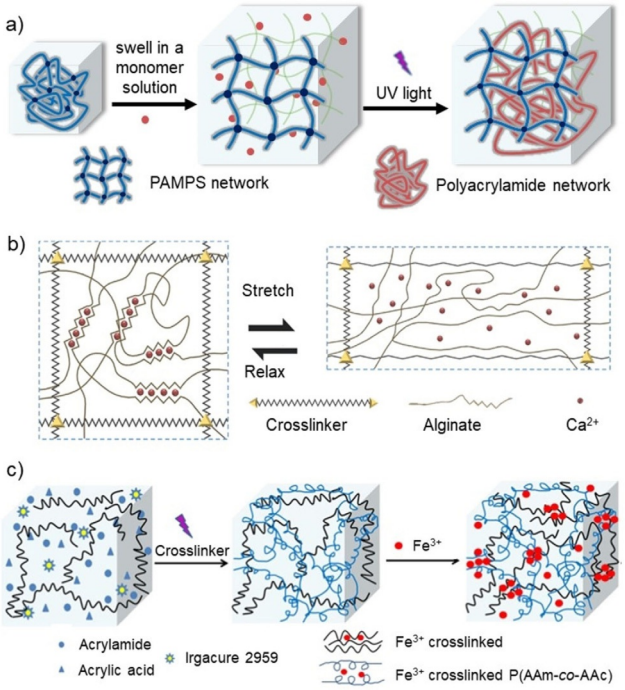

Figure 9. a) Synthetic illustration of the formation of a PAMPS/polyacrylamide double network hydrogel by soaking a PAMPS network in an acrylamide solution to form polyacrylamide after UV curing. b) Illustration of a supramolecular and covalent double network hydrogel formed by an alginate–Ca^{2+} complex and a photo-cross-linked PEG. Reproduced with permission from reference [118]. Copyright 2015 John Wiley & Sons, Inc. c) A double supramolecular network hydrogel formed by alginate/Fe^{3+} and poly(acrylamide-co-acrylic acid)/Fe^{3+} complexes by using a one-step double ionic cross-linking strategy wherein cross-linking is established by Fe^{3+} coordination with the carboxylic groups of SA and P(AAm-co-AAc). Reproduced with permission from reference [119]. Copyright 2018 American Chemical Society.

3. Reinforcing the mechanical properties of 3D printing polymers

The viscoelastic polymers used for DIW often possess limited mechanical strength and are fatigued by repeated mechanical stress, thus, improving their mechanical properties will greatly expand their applications.[113] Gong et al. originally introduced[114,115] the concept of a double network, which possesses significantly improved mechanical performance. To introduce the double network architecture, Wiley et al. developed[116] a two-step method to fabricate a DIW-based double network material with a cross-linked poly(2-acrylamido-2-methylpropanesulfonate) (PAMPS) network and another cross-linked polyacrylamide network. An extrudable ink was first prepared by mixing the AMPS monomer *N*,*N*′-methylenebis(acrylamide) cross-linker and the rheology modifier Laponite RDS. After DIW, the ink was quickly cross-linked under UV light. The monolith was then swelled in a solution of acrylamide monomers and cross-linkers followed by a second photo-cross-linking to generate the double covalently cross-linked double network monolith (Figure 9a).

Instead of a double covalent network, Spinks et al. integrated an alginate–Ca^{2+} supramolecular network with a cross-linked acrylamide network to increase the toughness of the 3D printed material.[117] In this ink, the alginate and acrylamide monomers were extruded, and their 3D scaffold was rigidified through photo-cross-linking. The supramolecularly cross-linked network was introduced by immersing the printed material into a Ca^{2+}-containing solution, affording the 3D printed double network material with a work of extension of 260 kJ m^{-3}. By replacing the short acrylamide cross-linker with a telechelic PEG-acrylate, Zhao et al. successfully imparted[118] good elasticity to the 3D printed double network material, which contains an alginate–Ca^{2+} supramolecular network and a covalent PEG network (Figure 9b). Apart from alginate, κ-carrageenan (a sulfated plant polysaccharide) has also been introduced to form supramolecular and covalent double network material. The κ-carrageenan can be thermally switched between the sol and gel state, which adds a thermal stimulus to tune the mechanical properties of the obtained double network material.

A double supramolecular network-based 3D printed monolith was fabricated by Li et al.[119] They constructed a dual coordination network hydrogel by using alginate/Fe^{3+} and poly(acrylamide-*co*-acrylic acid)/Fe^{3+}. The ink was prepared by mixing a solution of sodium alginate, acrylamide and acrylate acid monomers, a photoinitiator, and a rheological modifier. After a post-extrusion photo-polymerization, the monolith was

soaked in an $Fe(NO_3)_3$ solution to establish the two coordination networks simultaneously (Figure 9c). The obtained double network hydrogel possesses high mechanical strength, toughness, and good healing capability upon pH switching.

It is worth noting that rheological modifiers were added to these inks to adjust their viscosity and post-printing polymerization was performed to maintain the 3D printed structure. This highlights the importance of developing rheologically tailored polymers as DIW inks, which will greatly simplify the materials design for the development of mechanically robust DIW materials.

4. Advanced materials fabricated by DIW

4.1 Biomimetic 4D printing

Inspired by the nastic motions triggered by anisotropic microstructures in botanical systems, Lewis et al. designed and fabricated 3D architectures that possess local and anisotropic swelling behaviors.[120] In this composite ink, high-aspect-ratio nano-fibrillated cellulose (NFC) is introduced to a mixture of *N*,*N*-dimethylacrylamide, a photoinitiator, and nanoclay. During the DIW, NFC fibers were aligned along the printing direction and the alignment was chemically preserved through photo-cross-linking. These stiff NFC fillers ($E > 100$ GPa) limit the hydrogel swelling along its longitude and the printed architectures display anisotropic swelling behavior. Anisotropic Young's moduli of $E = 40$ kPa (longitudinal) and $E = 20$ kPa (transverse) were recorded in the cross-linked gel. This anisotropic swelling behavior was precisely engineered by designing the printing path, affording floral structures that twist upon swelling in water (Figure 10a).

4.2 Shape memory polymers

Recently, Qi et al. reported[121] the additive manufacturing of a stretchable shape memory material. The solvent-free printing ink is composed of an *n*-butyl acrylate monomer, a diacrylate cross-linker, a photo-initiator, a semicrystalline polycaprolactone (PCL), and a rheology modifier. To allow smooth extrusion, the ink was heated to 70 °C to disrupt the crystallization of the PCL. Each printed pattern is photo-cross-linked under UV irradiation. The printed monolith contains a cross-linked polyacrylate network and an interpenetrated PCL crystalline network. When the monolith is heated above the melting temperature (68 °C) of the PCL, the elastomer was mechanically folded to a temporary shape and kept still after cooling. The as-printed shape was recovered after reheating the elastomer above the melting point of the PCL and cooling down. Moreover, the semicrystalline PCL network also imparted stretchability to the monolith, exhibiting a fracture strain of 500–600% (Figure 10b).

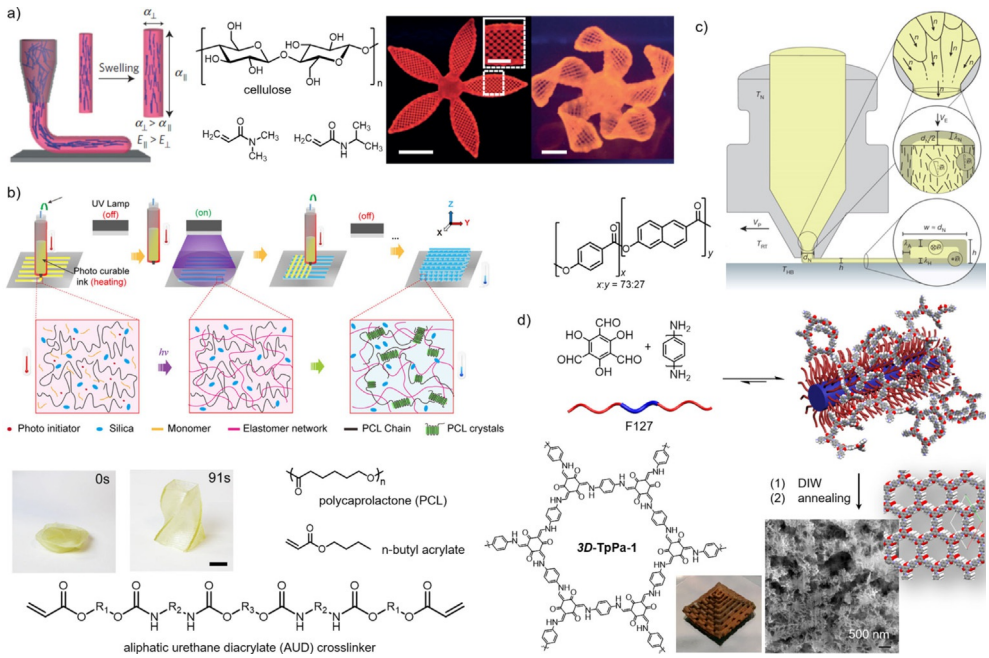

Figure 10. a) Anisotropic swelling of the printed monolith driven by locally aligned nano-fibrillated cellulose (NFC) formulated in the printing ink (scale bars: 5 mm, inset: 2.5 mm). Reproduced with permission from reference [120]. Copyright 2016 Macmillan Publishers, Nature. b) Shape memory polymers made of aliphatic urethane diacrylate, *n*-butyl acrylate, and semicrystalline polycaprolactone (scale bar: 6 mm). Reproduced with permission from reference [121]. Copyright 2018 American Chemical Society. c) Thermal extrusion of liquid–crystalline polymers onto a cooled printing stage. Accelerated cooling at the filament surface results in the formation of a core/shell polymer with ordered liquid–crystalline domains comprising the shell structure. Reproduced with permission from reference [123]. Copyright 2018 Macmillan Publishers, Nature. d) Fabrication of a 3D printed COF monolith. An imine polymer co-assembled with F127, forming homogenous hydrogel for DIW. The 3D printed monolith was annealed to allow an amorphous-to-crystalline transformation. Reproduced with permission from reference [124]. Copyright 2018 American Chemical Society.

4.3 Hierarchically ordered material

Controlling the structure of 3D printing polymers across the nano- to macroscale produces hierarchically ordered 3D printing materials with emergent properties. By using the hierarchical co-assembly-enhanced DIW method, we have successfully fabricated hierarchically porous 3D silica monoliths and fluorescent organosilica lattices.[76] In a similar manner, Biener et al. demonstrated[122] the 3D printing of a hierarchical porous gold monolith. An Ag–Au composite ink composed of Ag and Au clays and melaleuca alternifolia (tea tree) leaf oil was 3D printed into a lattice cube. After post-printing calcination and chemical etching of Ag, the as-printed monolith was converted to a hierarchical porous Ag–Au alloyed monolith.

Studart et al. demonstrated[123] a 3D printing approach to prepare materials with hierarchical core–shell architecture by using liquid crystalline polymers. A rigid aromatic polyester consisting of *p*-hydroxybenzoic and 2-hydroxy-6-naphthoic repeating units was extruded from the heated printing nozzle (Figure 10 c). The mechanical shear force aligned the nematic domains of the polymer in the direction of the flow. Considering that the polymers were cooled down faster at the surface, their flow-aligned nematic order was well preserved, whereas the polymer at the interior adopts a more random order due to slower cooling. The filament diameter and the printing temperature affected the thickness of the ordered shell, which subsequently altered the Young's modulus of the printed filaments. When the printed filaments were thermally annealed, additional polycondensation took place orthogonally to the direction of the polymer alignment, further strengthening the mechanical properties of the filament and affording one of the strongest 3D printed polymer materials.

Annealing 3D printed polymer monoliths have also been demonstrated to fabricate hierarchically ordered, highly crystalline porous covalent organic framework (COF) materials (Figure 10 d).[124] We introduced pluronic F127 as a 3D printing template to co-assemble with imine polymers in an aqueous environment. By limiting the degree of imine polycondensation, the amorphous imine polymer and F127 form co-assembled hydrogels with suitable shear-thinning and rapid self-healing properties for DIW. The amorphous 3D printed monolith was then heated to extensively polymerize the imine network. After the removal of the F127 template followed by an amorphous-to-crystalline annealing process, three COFs have been fabricated into 3D monoliths, possessing high crystallinity, hierarchical pores with high surface areas as well as good structural integrity, and robust mechanical stability. When multiple inks are employed for DIW, heterogeneous dual-component COF monoliths are fabricated with high spatial precision.

4.4 Smart materials operated by molecular motions

Living systems are able to achieve sophisticated tasks through a cascade of dynamic molecular events performed in a synchronized and hierarchically organized manner. Limited by the random distributions and orientations, synthetic polymers that can cohesively amplify molecular-level functions to the macroscopic level are still elusive. Designing 3D printable polymer materials that can transfer molecular level functions to the macroscale not only accelerates the development of stimuli-responsive polymers at the fundamental level, but also promotes the design of advanced architectures with optimized spatial variation at the macroscale to perform complex tasks.

By facilitating the 3D printability of CD-based polypseudorotaxanes through microcrystallization, we designed a series of 3D polyrotaxanes that amplify the CD ring shuttling motions to the macroscale and perform useful mechanical work.[89] In an aqueous environment, the CD rings are hydrogen bonded to form static microcrystalline domains in the polyrotaxane monolith. When DMSO is introduced, the hydrogen-bonding network formed between the CD rings is disrupted. The CD rings randomly shuttle along the PEG chain and the 3D printed monolith loses its as-designed shape. When water is reintroduced, the CD rings are switched from the shuttling state to stationary state, and the printed hydrogel recovers its as-printed shape and is capable of lifting aluminum plates against gravity (Figure 11 a). It is important to note that the solvent diffusion problem is largely mitigated in the 3D printed lattice cube benefiting from the multiple diffusion pathways of the macroscopic voids. Later, we reported a pH-operated 3D printed polyrotaxane material with a faster response compared to the solvent-responsive system.[90] The (de)protonation of the hydroxyl groups of the CDs in the polyrotaxanes enabled a fast switching between the shuttling and stationary states, affording rapid macroscopic working cycles upon pH variation. By conjugating this pH-operated polyrotaxane material with acrylic polymers, the printed material exhibits a two-stage pH-induced shape-changing behavior. When these materials are printed heterogeneously through dual-material DIW, the printed monolith exhibits complex multi-stage anisotropic shape morphing at different pH (Figure 11 b).

Other than switching the rings in polyrotaxanes, switching the liquid crystalline polymers between a randomly oriented amorphous phase and a highly ordered liquid crystalline phase can also amplify the molecular motions to the macroscopic scale. For example, anisotropic mechanical properties can be achieved by aligning thermotropic liquid crystalline polymers between the nematic-isotropic temperature T_{NI} and the glass transition temperature T_g ($T_g < T_{NI}$).[125] When a solvent-free liquid crystal elastomer ink composed of a mixture of mesogen oligomers and photo-initiators was 3D printed, these liquid crystalline polymers in the nematic phase are mechanically aligned upon shearing and chemically locked through photo-cross-linking. The spatial control of the directional alignment of the ink enables the printed monolith to undergo complex reversible shape transformations. For example, a disk printed with layered spiral and perpendicular meandering printing pathways morphs into a saddle form upon heating and snaps into an inverted saddle form upon cooling, exhibiting reversible 3D-to-3D shape transformation (Figure 11 c).

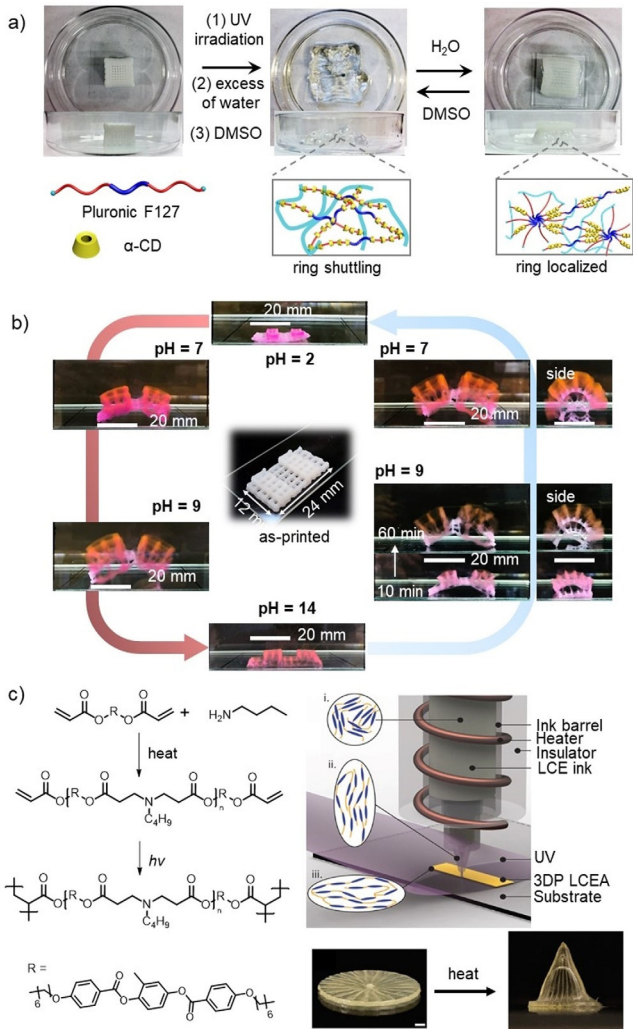

Figure 11. a) Images of a wood-pile polyrotaxane lattice soaked in DMSO and water, respectively. Reproduced with permission from reference [89]. Copyright 2017 John Wiley & Sons, Inc. b) pH-Induced multi-stage anisotropic shape morphing of a 3D printed polyrotaxane-based hybrid. A polyrotaxane-co-polyacrylic acid layer is fabricated on top of a polyrotaxane lattice. Reproduced with permission from reference [90]. Copyright 2018 The Royal Society of Chemistry. c) A liquid crystalline oligomer ink synthesized by an aza-Michael addition was 3D printed into a layered disc architecture followed by photo-polymerization. The disc morphed to cone shape upon heating as a result of the nematic-to-amorphous phase transition (scale bar: 1 mm). Reproduced with permission from reference [125]. Copyright 2018 John Wiley & Sons, Inc.

5. Conclusion and Outlook

It is clear that developing advanced polymers tailored for specific 3D printing systems will greatly accelerate the development of additive manufacturing. Synthesizing polymers with suitable rheological properties that can be self-supportive after direct ink writing is highly desired. Compared to the rapid progress made in the development of DIW inks through engineering approaches, bottom-up syntheses of molecular and polymeric systems for direct ink writing has started to draw the attention of chemists only recently.

From a molecular design perspective, intensively investigated block copolymer phase segregation[68,69,126–128] is a promising path to design DIW polymers. Furthermore, the rich toolbox containing a variety of supramolecular binding motifs could also be transferred for the development of DIW inks. To date, only a few of them including the alginate–Ca^{2+} complex, cyclodextrin-based polyrotaxanes and host–guest complexes, and amphiphilic polymers have been employed for DIW polymer design. We envision that multivalent hydrogen-bonding donor–acceptor arrays[129] and cucurbituril-based host–guest complexes[130,131] are also promising for DIW polymer design owing to their small kinetic dissociation constants. One of the biggest challenges, as well as an exciting opportunity, in the development of DIW polymers lies in amplifying the designed molecular functions to the macroscale. The hierarchical control of polymers across the nano- to macroscale requires both experimental exploration and computational simulation.

From a materials development perspective, introducing functional polymers to DIW will enable the development and hetero-integration of stimuli-responsive materials and devices. Coupled with digital design, we will be able to program complex functions with high spatial and temporal control. Novel DIW ink design will also enable the additive manufacturing of emergent materials, such as perovskites for energy-related applications and porous materials for separation and catalysis, etc.

From a technology perspective, the development of DIW polymers will greatly improve the printing speed of DIW, because both the in situ and post-printing cross-linking of injectable (or extrudable) inks are constrained by the rate of photopolymerization, not to mention both methods add complexity and cost to the 3D printing system. It also shows promise in enhancing the 3D printing resolution. Furthermore, an expanded library of DIW polymers will enable scientists to take advantage of different material properties to digitally design meta-materials with emergent mechanical properties for the development of tissue engineering and soft robotics.

Overall, the convergence of advanced polymer design, the development of the direct ink writing platform, and advanced digital simulation will enable the fabrication of smart materials and devices beyond our current reach.

Acknowledgements

We acknowledge the funding support from Dartmouth College and NSF EPSCoR New Hampshire Bio-Made Center (no. 1757371). C.K. thanks the support of Cottrell Scholar Award (no. 25877) from the Research Corporation for Science Advancement.

Conflict of interest

The authors declare no conflict of interest.

Keywords: 3D printing · direct ink writing · polymers · rheology · supramolecular chemistry

[1] R. L. Truby, J. A. Lewis, *Nature* **2016**, *540*, 371 – 378.
[2] S. C. Ligon, R. Liska, J. Stampfl, M. Gurr, R. Mülhaupt, *Chem. Rev.* **2017**, *117*, 10212 – 10290.
[3] S. S. Crump, Apparatus and Method for Creating Three-Dimensional Objects, US5121329A, **1992**.
[4] G. A. Appuhamillage, J. C. Reagan, S. Khorsandi, J. R. Davidson, W. Voit, R. A. Smaldone, *Polym. Chem.* **2017**, *8*, 2087 – 2092.
[5] K. Yang, J. C. Grant, P. Lamey, A. Joshi-Imre, B. R. Lund, R. A. Smaldone, W. Voit, *Adv. Funct. Mater.* **2017**, *27*, 1700318.
[6] M. A. Luzuriaga, D. R. Berry, J. C. Reagan, R. A. Smaldone, J. J. Gassensmith, *Lab Chip* **2018**, *18*, 1223 – 1230.
[7] C. W. Hull, Apparatus for Production of Three-Dimensional Objects by Stereolithography, US4575330A, **1986**.
[8] C. R. Deckard, Method and Apparatus for Producing Parts by Selective Sintering, US4863538A, **1989**.
[9] "Wohlers Associates Publishes 23rd Edition of Its 3D Printing and Additive Manufacturing Industry Report | Wohlers Associates," can be found under https://wohlersassociates.com/press74.html.
[10] T.-H. Chen, S. Lee, A. H. Flood, O. Š. Miljanić, *CrystEngComm* **2014**, *16*, 5488 – 5493.
[11] M. Attaran, *Bus. Horiz.* **2017**, *60*, 677 – 688.
[12] I. Gibson, D. Rosen, B. Stucker, *Additive Manufacturing Technologies: 3D Printing, Rapid Prototyping, and Direct Digital Manufacturing*, Springer, New York, **2015**.
[13] J. R. Tumbleston, D. Shirvanyants, N. Ermoshkin, R. Januszіéwicz, A. R. Johnson, D. Kelly, K. Chen, R. Pinschmidt, J. P. Rolland, A. Ermoshkin, E. T. Samulski, J. M. DeSimone, *Science* **2015**, *347*, 1349 – 1352.
[14] O. S. Carneiro, A. F. Silva, R. Gomes, *Mater. Des.* **2015**, *83*, 768 – 776.
[15] T. J. Hinton, Q. Jallerat, R. N. Palchesko, J. H. Park, M. S. Grodzicki, H.-J. Shue, M. H. Ramadan, A. R. Hudson, A. W. Feinberg, *Sci. Adv.* **2015**, *1*, e1500758.
[16] J. Malda, J. Visser, F. P. Melchels, T. Jüngst, W. E. Hennink, W. J. A. Dhert, J. Groll, D. W. Hutmacher, *Adv. Mater.* **2013**, *25*, 5011 – 5028.
[17] B. Xie, R. L. Parkhill, W. L. Warren, J. E. Smay, *Adv. Funct. Mater.* **2006**, *16*, 1685 – 1693.
[18] Y. S. Zhang, A. Khademhosseini, *Science* **2017**, *356*, eaaf3627.
[19] Y. S. Zhang, K. Yue, J. Aleman, K. Mollazadeh-Moghaddam, S. M. Bakht, J. Yang, W. Jia, V. Dell'Erba, P. Assawes, S. R. Shin, M. R. Dokmeci, R. Oklu, A. Khademhosseini, *Ann. Biomed. Eng.* **2017**, *45*, 148 – 163.
[20] M. Wehner, R. L. Truby, D. J. Fitzgerald, B. Mosadegh, G. M. Whitesides, J. A. Lewis, R. J. Wood, *Nature* **2016**, *536*, 451 – 455.
[21] M. Cianchetti, C. Laschi, A. Menciassi, P. Dario, *Nat. Rev. Mater.* **2018**, *3*, 143 – 153.
[22] L. Yu, J. Ding, *Chem. Soc. Rev.* **2008**, *37*, 1473 – 1481.
[23] P. Y. W. Dankers, T. M. Hermans, T. W. Baughman, Y. Kamikawa, R. E. Kieltyka, M. M. C. Bastings, H. M. Janssen, N. A. J. M. Sommerdijk, A. Larsen, M. J. A. van Luyn, A. W. Bosman, E. R. Popa, G. Fytas, E. W. Meijer, *Adv. Mater.* **2012**, *24*, 2703 – 2709.
[24] M. J. Webber, E. A. Appel, E. W. Meijer, R. Langer, *Nat. Mater.* **2016**, *15*, 13 – 26.
[25] J. A. Lewis, *Adv. Funct. Mater.* **2006**, *16*, 2193 – 2204.
[26] K. Hölzl, S. Lin, L. Tytgat, S. Van Vlierberghe, L. Gu, A. Ovsianikov, *Biofabrication* **2016**, *8*, 032002.
[27] N. Paxton, W. Smolan, T. Böck, F. Melchels, J. Groll, T. Jungst, *Biofabrication* **2017**, *9*, 044107.
[28] D. Y. Wu, S. Meure, D. Solomon, *Prog. Polym. Sci.* **2008**, *33*, 479 – 522.
[29] M. Burnworth, L. Tang, J. R. Kumpfer, A. J. Duncan, F. L. Beyer, G. L. Fiore, S. J. Rowan, C. Weder, *Nature* **2011**, *472*, 334 – 337.
[30] A. Campanella, D. Döhler, W. H. Binder, *Macromol. Rapid Commun.* **2018**, *39*, 1700739.
[31] A. B. Metzner, *J. Rheol.* **1985**, *29*, 739 – 775.
[32] M. Guvendiren, H. D. Lu, J. A. Burdick, *Soft Matter* **2012**, *8*, 260 – 272.
[33] D. T. N. Chen, Q. Wen, P. A. Janmey, J. C. Crocker, A. G. Yodh, *Annu. Rev. Condens. Matter Phys.* **2010**, *1*, 301 – 322.
[34] J. Swenson, M. V. Smalley, H. L. M. Hatharasinghe, *Phys. Rev. Lett.* **1998**, *81*, 5840 – 5843.
[35] C. Maffi, M. Baiesi, L. Casetti, F. Piazza, P. De Los Rios, *Nat. Commun.* **2012**, *3*, 1065.
[36] O. Kretschmann, S. W. Choi, M. Miyauchi, I. Tomatsu, A. Harada, H. Ritter, *Angew. Chem. Int. Ed.* **2006**, *45*, 4361 – 4365; *Angew. Chem.* **2006**, *118*, 4468 – 4472.
[37] E. A. Appel, J. del Barrio, X. J. Loh, O. A. Scherman, *Chem. Soc. Rev.* **2012**, *41*, 6195 – 6214.
[38] X. Ji, Y. Yao, J. Li, X. Yan, F. Huang, *J. Am. Chem. Soc.* **2013**, *135*, 74 – 77.
[39] J. B. Beck, S. J. Rowan, *J. Am. Chem. Soc.* **2003**, *125*, 13922 – 13923.
[40] S. C. Grindy, R. Learsch, D. Mozhdehi, J. Cheng, D. G. Barrett, Z. Guan, P. B. Messersmith, N. Holten-Andersen, *Nat. Mater.* **2015**, *14*, 1210 – 1216.
[41] Y.-L. Rao, A. Chortos, R. Pfattner, F. Lissel, Y.-C. Chiu, V. Feig, J. Xu, T. Kurosawa, X. Gu, C. Wang, M. He, J. W. Chung, Z. Bao, *J. Am. Chem. Soc.* **2016**, *138*, 6020 – 6027.
[42] C. T. Seto, G. M. Whitesides, *J. Am. Chem. Soc.* **1993**, *115*, 905 – 916.
[43] S. Burattini, B. W. Greenland, D. H. Merino, W. Weng, J. Seppala, H. M. Colquhoun, W. Hayes, M. E. Mackay, I. W. Hamley, S. J. Rowan, *J. Am. Chem. Soc.* **2010**, *132*, 12051 – 12058.
[44] M. Guo, L. M. Pitet, H. M. Wyss, M. Vos, P. Y. W. Dankers, E. W. Meijer, *J. Am. Chem. Soc.* **2014**, *136*, 6969 – 6977.
[45] C. F. J. Faul, M. Antonietti, *Adv. Mater.* **2003**, *15*, 673 – 683.
[46] F. Shi, Z. Wang, X. Zhang, *Adv. Mater.* **2005**, *17*, 1005 – 1009.
[47] I. Willerich, F. Gröhn, *Angew. Chem. Int. Ed.* **2010**, *49*, 8104 – 8108; *Angew. Chem.* **2010**, *122*, 8280 – 8285.
[48] H. J. Schneider, T. Schiestel, P. Zimmermann, *J. Am. Chem. Soc.* **1992**, *114*, 7698 – 7703.
[49] K. Tahara, S. Lei, J. Adisoejoso, S. D. Feyter, Y. Tobe, *Chem. Commun.* **2010**, *46*, 8507 – 8525.
[50] M. Yoshizawa, T. Kusukawa, M. Kawano, T. Ohhara, I. Tanaka, K. Kurihara, N. Niimura, M. Fujita, *J. Am. Chem. Soc.* **2005**, *127*, 2798 – 2799.
[51] T. Kakuta, Y. Takashima, M. Nakahata, M. Otsubo, H. Yamaguchi, A. Harada, *Adv. Mater.* **2013**, *25*, 2849 – 2853.
[52] L. J. Dooling, D. A. Tirrell, *ACS Cent. Sci.* **2016**, *2*, 812 – 819.
[53] J. L. Dávila, M. A. d'Ávila, *Int. J. Adv. Manuf. Technol.* **2019**, *101*, 675 – 686.
[54] G. Siqueira, D. Kokkinis, R. Libanori, M. K. Hausmann, A. S. Gladman, A. Neels, P. Tingaut, T. Zimmermann, J. A. Lewis, A. R. Studart, *Adv. Funct. Mater.* **2017**, *27*, 1604619.
[55] A. G. Tabriz, M. A. Hermida, N. R. Leslie, W. Shu, *Biofabrication* **2015**, *7*, 045012.
[56] C. B. Highley, C. B. Rodell, J. A. Burdick, *Adv. Mater.* **2015**, *27*, 5075 – 5079.
[57] L. Ouyang, C. B. Highley, C. B. Rodell, W. Sun, J. A. Burdick, *ACS Biomater. Sci. Eng.* **2016**, *2*, 1743 – 1751.
[58] L. Ouyang, C. B. Highley, W. Sun, J. A. Burdick, *Adv. Mater.* **2017**, *29*, 1604983.
[59] J. D. Badjić, A. Nelson, S. J. Cantrill, W. B. Turnbull, J. F. Stoddart, *Acc. Chem. Res.* **2005**, *38*, 723 – 732.
[60] C. A. Hunter, H. L. Anderson, *Angew. Chem. Int. Ed.* **2009**, *48*, 7488 – 7499; *Angew. Chem.* **2009**, *121*, 7624 – 7636.
[61] M. Du, B. Chen, Q. Meng, S. Liu, X. Zheng, C. Zhang, H. Wang, H. Li, N. Wang, J. Dai, *Biofabrication* **2015**, *7*, 044104.
[62] S. Kyle, Z. M. Jessop, A. Al-Sabah, I. S. Whitaker, *Adv. Healthcare Mater.* **2017**, *6*, 1700264.
[63] L. Maibaum, A. R. Dinner, D. Chandler, *J. Phys. Chem. B* **2004**, *108*, 6778 – 6781.
[64] B. Jeong, Y. H. Bae, S. W. Kim, *Macromolecules* **1999**, *32*, 7064 – 7069.
[65] C. Chaibundit, N. M. P. S. Ricardo, F. M. L. L. Costa, S. G. Yeates, C. Booth, *Langmuir* **2007**, *23*, 9229 – 9236.
[66] G. A. Appuhamillage, D. R. Berry, C. E. Benjamin, M. A. Luzuriaga, J. C. Reagan, J. J. Gassensmith, R. A. Smaldone, *Polym. Int.* **2019**, *68*, 964 – 971.
[67] X. Liu, H. Yuk, S. Lin, G. A. Parada, T.-C. Tang, E. Tham, C. de la Fuente-Nunez, T. K. Lu, X. Zhao, *Adv. Mater.* **2018**, *30*, 1704821.
[68] M. Zhang, A. Vora, W. Han, R. J. Wojtecki, H. Maune, A. B. A. Le, L. E. Thompson, G. M. McClelland, F. Ribet, A. C. Engler, A. Nelson, *Macromolecules* **2015**, *48*, 6482 – 6488.
[69] D. G. Karis, R. J. Ono, M. Zhang, A. Vora, D. Storti, M. A. Ganter, A. Nelson, *Polym. Chem.* **2017**, *8*, 4199 – 4206.
[70] G.-E. Yu, Y. Deng, S. Dalton, Q.-G. Wang, D. Attwood, C. Price, C. Booth, *J. Chem. Soc. Faraday Trans.* **1992**, 2537 – 2544.
[71] W. Wu, A. DeConinck, J. A. Lewis, *Adv. Mater.* **2011**, *23*, H178 – H183.
[72] R. L. Truby, M. Wehner, A. K. Grosskopf, D. M. Vogt, S. G. M. Uzel, R. J. Wood, J. A. Lewis, *Adv. Mater.* **2018**, *30*, 1706383.

[73] N. Y. C. Lin, K. A. Homan, S. S. Robinson, D. B. Kolesky, N. Duarte, A. Moisan, J. A. Lewis, *Proc. Natl. Acad. Sci. USA* **2019**, *116*, 5399 – 5404.
[74] D. Zhao, J. Feng, Q. Huo, N. Melosh, G. H. Fredrickson, B. F. Chmelka, G. D. Stucky, *Science* **1998**, *279*, 548 – 552.
[75] G. Pérez-Sánchez, S.-C. Chien, J. R. B. Gomes, M. N. D. S. Cordeiro, S. M. Auerbach, P. A. Monson, M. Jorge, *Chem. Mater.* **2016**, *28*, 2715 – 2727.
[76] L. Li, P. Zhang, Z. Zhang, Q. Lin, Y. Wu, A. Cheng, Y. Lin, C. M. Thompson, R. A. Smaldone, C. Ke, *Angew. Chem. Int. Ed.* **2018**, *57*, 5105 – 5109; *Angew. Chem.* **2018**, *130*, 5199 – 5203.
[77] M. Zhang, D. Xu, X. Yan, J. Chen, S. Dong, B. Zheng, F. Huang, *Angew. Chem. Int. Ed.* **2012**, *51*, 7011 – 7015; *Angew. Chem.* **2012**, *124*, 7117 – 7121.
[78] F. Herbst, D. Döhler, P. Michael, W. H. Binder, *Macromol. Rapid Commun.* **2013**, *34*, 203 – 220.
[79] K. Miyamae, M. Nakahata, Y. Takashima, A. Harada, *Angew. Chem. Int. Ed.* **2015**, *54*, 8984 – 8987; *Angew. Chem.* **2015**, *127*, 9112 – 9115.
[80] J. Jia, D. J. Richards, S. Pollard, Y. Tan, J. Rodriguez, R. P. Visconti, T. C. Trusk, M. J. Yost, H. Yao, R. R. Markwald, Y. Mei, *Acta Biomater.* **2014**, *10*, 4323 – 4331.
[81] E. Axpe, M. L. Oyen, *Int. J. Mol. Sci.* **2016**, *17*, 1976.
[82] Y. Yan, H. Yang, F. Zhang, B. Tu, D. Zhao, *Small* **2006**, *2*, 517 – 521.
[83] C. E. Boott, J. Gwyther, R. L. Harniman, D. W. Hayward, I. Manners, *Nat. Chem.* **2017**, *9*, 785 – 792.
[84] H. Wang, J. K. Keum, A. Hiltner, E. Baer, B. Freeman, A. Rozanski, A. Galeski, *Science* **2009**, *323*, 757 – 760.
[85] B. Yu, X. Jiang, J. Yin, *Macromolecules* **2014**, *47*, 4761 – 4768.
[86] X. Wang, G. Guerin, H. Wang, Y. Wang, I. Manners, M. A. Winnik, *Science* **2007**, *317*, 644 – 647.
[87] H. Qiu, Z. M. Hudson, M. A. Winnik, I. Manners, *Science* **2015**, *347*, 1329 – 1332.
[88] Z. Lei, Q. Wang, P. Wu, *Mater. Horiz.* **2017**, *4*, 694 – 700.
[89] Q. Lin, X. Hou, C. Ke, *Angew. Chem. Int. Ed.* **2017**, *56*, 4452 – 4457; *Angew. Chem.* **2017**, *129*, 4523 – 4528.
[90] Q. Lin, L. Li, M. Tang, X. Hou, C. Ke, *J. Mater. Chem. C* **2018**, *6*, 11956 – 11960.
[91] S. Kamitori, O. Matsuzaka, S. Kondo, S. Muraoka, K. Okuyama, K. Noguchi, M. Okada, A. Harada, *Macromolecules* **2000**, *33*, 1500 – 1502.
[92] S. J. Rowan, S. J. Cantrill, G. R. L. Cousins, J. K. M. Sanders, J. F. Stoddart, *Angew. Chem. Int. Ed.* **2002**, *41*, 898 – 952; *Angew. Chem.* **2002**, *114*, 938 – 993.
[93] T. Maeda, H. Otsuka, A. Takahara, *Prog. Polym. Sci.* **2009**, *34*, 581 – 604.
[94] M. Nadgorny, Z. Xiao, L. A. Connal, *Mol. Syst. Des. Eng.* **2017**, *2*, 283 – 292.
[95] M. Nadgorny, J. Collins, Z. Xiao, P. J. Scales, L. A. Connal, *Polym. Chem.* **2018**, *9*, 1684 – 1692.
[96] L. L. Wang, C. B. Highley, Y.-C. Yeh, J. H. Galarraga, S. Uman, J. A. Burdick, *J. Biomed. Mater. Res. Part A* **2018**, *106*, 865 – 875.
[97] Q. Wei, W. Xu, Q. Zhang, S. Zhang, L. Cheng, Q. Wang, *J. Mater. Chem. B* **2017**, *5*, 5092 – 5095.
[98] L. L. Lebel, B. Aissa, M. A. E. Khakani, D. Therriault, *Adv. Mater.* **2010**, *22*, 592 – 596.
[99] A. Skardal, J. Zhang, L. McCoard, X. Xu, S. Oottamasathien, G. D. Prestwich, *Tissue Eng. Part A* **2010**, *16*, 2675 – 2685.
[100] L. A. Hockaday, K. H. Kang, N. W. Colangelo, P. Y. C. Cheung, B. Duan, E. Malone, J. Wu, L. N. Girardi, L. J. Bonassar, H. Lipson, C. C. Chu, J. T. Butcher, *Biofabrication* **2012**, *4*, 035005.
[101] R. F. Pereira, P. J. Bártolo, *J. Appl. Polym. Sci.* **2015**, *132*, 42458.
[102] D. A. Rau, J. Herzberger, T. E. Long, C. B. Williams, *ACS Appl. Mater. Interfaces* **2018**, *10*, 34828 – 34833.
[103] I. D. Robertson, M. Yourdkhani, P. J. Centellas, J. E. Aw, D. G. Ivanoff, E. Goli, E. M. Lloyd, L. M. Dean, N. R. Sottos, P. H. Geubelle, J. S. Moore, S. R. White, *Nature* **2018**, *557*, 223 – 227.
[104] S. P. Davtyan, P. V. Zhirkov, S. A. Vol'fson, *Russ. Chem. Rev.* **1984**, *53*, 150 – 163.
[105] I. D. Robertson, E. L. Pruitt, J. S. Moore, *ACS Macro Lett.* **2016**, *5*, 593 – 596.
[106] I. D. Robertson, L. M. Dean, G. E. Rudebusch, N. R. Sottos, S. R. White, J. S. Moore, *ACS Macro Lett.* **2017**, *6*, 609 – 612.
[107] C. S. O'Bryan, T. Bhattacharjee, S. Hart, C. P. Kabb, K. D. Schulze, I. Chilakala, B. S. Sumerlin, W. G. Sawyer, T. E. Angelini, *Sci. Adv.* **2017**, *3*, e1602800.
[108] G. M. Gratson, M. Xu, J. A. Lewis, *Nature* **2004**, *428*, 386.
[109] M. Costantini, C. Colosi, W. Święszkowski, A. Barbetta, *Biofabrication* **2018**, *11*, 012001.
[110] F. Zhu, L. Cheng, J. Yin, Z. L. Wu, J. Qian, J. Fu, Q. Zheng, *ACS Appl. Mater. Interfaces* **2016**, *8*, 31304 – 31310.
[111] J. Forth, X. Liu, J. Hasnain, A. Toor, K. Miszta, S. Shi, P. L. Geissler, T. Emrick, B. A. Helms, T. P. Russell, *Adv. Mater.* **2018**, *30*, 1707603.
[112] M. Cui, T. Emrick, T. P. Russell, *Science* **2013**, *342*, 460 – 463.
[113] S. A. M. Tofail, E. P. Koumoulos, A. Bandyopadhyay, S. Bose, L. O'Donoghue, C. Charitidis, *Mater. Today* **2018**, *21*, 22 – 37.
[114] J. P. Gong, Y. Katsuyama, T. Kurokawa, Y. Osada, *Adv. Mater.* **2003**, *15*, 1155 – 1158.
[115] J. P. Gong, *Soft Matter* **2010**, *6*, 2583 – 2590.
[116] F. Yang, V. Tadepalli, B. J. Wiley, *ACS Biomater. Sci. Eng.* **2017**, *3*, 863 – 869.
[117] S. E. Bakarich, M. I. H. Panhuis, S. Beirne, G. G. Wallace, G. M. Spinks, *J. Mater. Chem. B* **2013**, *1*, 4939 – 4946.
[118] S. Hong, D. Sycks, H. F. Chan, S. Lin, G. P. Lopez, F. Guilak, K. W. Leong, X. Zhao, *Adv. Mater.* **2015**, *27*, 4035 – 4040.
[119] X. Li, H. Wang, D. Li, S. Long, G. Zhang, Z. Wu, *ACS Appl. Mater. Interfaces* **2018**, *10*, 31198 – 31207.
[120] A. S. Gladman, E. A. Matsumoto, R. G. Nuzzo, L. Mahadevan, J. A. Lewis, *Nat. Mater.* **2016**, *15*, 413 – 418.
[121] X. Kuang, K. Chen, C. K. Dunn, J. Wu, V. C. F. Li, H. J. Qi, *ACS Appl. Mater. Interfaces* **2018**, *10*, 7381 – 7388.
[122] C. Zhu, Z. Qi, V. A. Beck, M. Luneau, J. Lattimer, W. Chen, M. A. Worsley, J. Ye, E. B. Duoss, C. M. Spadaccini, C. M. Friend, J. Biener, *Sci. Adv.* **2018**, *4*, eaas9459.
[123] S. Gantenbein, K. Masania, W. Woigk, J. P. W. Sesseg, T. A. Tervoort, A. R. Studart, *Nature* **2018**, *561*, 226 – 230.
[124] M. Zhang, L. Li, Q. Lin, M. Tang, Y. Wu, C. Ke, *J. Am. Chem. Soc.* **2019**, *141*, 5154 – 5158.
[125] A. Kotikian, R. L. Truby, J. W. Boley, T. J. White, J. A. Lewis, *Adv. Mater.* **2018**, *30*, 1706164.
[126] Y. Mai, A. Eisenberg, *Chem. Soc. Rev.* **2012**, *41*, 5969 – 5985.
[127] A. Abbadessa, M. Landín, E. O. Blenke, W. E. Hennink, T. Vermonden, *Eur. Polym. J.* **2017**, *92*, 13 – 26.
[128] R. T. Shafranek, S. C. Millik, P. T. Smith, C.-U. Lee, A. J. Boydston, A. Nelson, *Prog. Polym. Sci.* **2019**, *93*, 36 – 67.
[129] F. H. Beijer, H. Kooijman, A. L. Spek, R. P. Sijbesma, E. W. Meijer, *Angew. Chem. Int. Ed.* **1998**, *37*, 75 – 78; *Angew. Chem.* **1998**, *110*, 79 – 82.
[130] S. Liu, C. Ruspic, P. Mukhopadhyay, S. Chakrabarti, P. Y. Zavalij, L. Isaacs, *J. Am. Chem. Soc.* **2005**, *127*, 15959 – 15967.
[131] J. Liu, C. S. Y. Tan, Z. Yu, N. Li, C. Abell, O. A. Scherman, *Adv. Mater.* **2017**, *29*, 1605325.

Manuscript received: March 1, 2019
Revised manuscript received: May 10, 2019
Accepted manuscript online: May 14, 2019
Version of record online: July 3, 2019